PERGAMON

Journal of Structural Geology 25 (2003) 557–574

JOURNAL OF STRUCTURAL GEOLOGY

www.elsevier.com/locate/jstrugeo

Strain localization due to a positive feedback of deformation and myrmekite-forming reaction in granite and aplite mylonites along the Hatagawa Shear Zone of NE Japan

Junko Tsurumi, Hiroko Hosonuma, Kyuichi Kanagawa*

Department of Earth Sciences, Chiba University, Chiba 263-8522, Japan

Received 22 February 2001; received in revised form 22 May 2001; accepted 22 March 2002

Abstract

With increasing mylonitization of aplite veins and their adjacent granite in the Hatagawa Shear Zone of NE Japan, the modal content and grain size of feldspar porphyroclasts decrease, while the modal content of fine-grained (≤ 50 μm) polymineralic aggregate of plagioclase, K-feldspar, quartz and biotite increases up to 60–80% in the granite and aplite ultramylonites. Deformation-induced myrmekite lobes are ubiquitously developed around K-feldspar porphyroclasts. The occurrence and chemical composition of plagioclase and K-feldspar in fine-grained polymineralic aggregates indicate that the plagioclase is mostly derived from myrmekite, while the interstitial K-feldspar originates from isolated porphyroclast rims between growing myrmekite lobes and/or precipitations from solution. Modal and bulk chemical compositions of granite and aplite indicate that the mylonites are preferentially developed in aplite veins richer in K-feldspar than the surrounding granite. Deformation-induced K-feldspar replacement by myrmekite is then more favored during deformation to produce more abundant fine-grained polymineralic aggregates. Subsequent reaction softening leads to more enhanced deformation, which promotes further myrmekite-forming reaction. Such a positive feedback of deformation and myrmekite-forming reaction in aplite veins and their adjacent granite may be responsible for strain localization in the granite and aplite mylonites along the Hatagawa Shear Zone.

Keywords: Strain localization; Granite; Aplite; Mylonite; Myrmekite forming reaction

1. Introduction

Ductile shear zones are regarded as localized zones of ductile shear strain in which strain softening has occurred (White et al., 1980). Several strain softening processes have been proposed: (1) dynamic recrystallization and associated grain-size reduction, (2) fabric softening due to preferred alignment of lattice planes for easy dislocation glide, (3) reaction softening, (4) physical and/or chemical effects of introduced water, and (5) shear heating (e.g. Poirier, 1980; White et al., 1980; Tullis et al., 1982; Tullis and Yund, 1985). Localized zones of strain softening may be rock layers with intrinsic lower strength than the surrounding layers. Examples include the Lochseiten limestone underlying the Glarus thrust (Schmid, 1975) and evaporites in décollements (Malavieille and Ritz, 1989). Or they may be pre-existing brittle shear zones or pseudotachylyte layers (e.g. Passchier, 1982; Segall and Simpson, 1986; Gibson, 1990; Tullis et al., 1990; Guermani and Pennacchioni, 1998; Takagi et al., 2000). However, ductile shear zones developed within a rock mass of similar lithology or those without brittle precursors are also common, and their strain localization processes are still poorly understood.

We describe in this paper a strain localization process in a granite along the Hatagawa Shear Zone of NE Japan. Changes with progressive mylonitization in microstructure, modal composition, grain size, quartz aggregate shape, quartz *c*-axis fabric, and bulk and mineral chemistries indicate that the mylonites are preferentially developed in aplite veins and their adjacent granite through a positive feedback of deformation and myrmekite-forming reaction. Such strain localization may be common in ductile shear zones in the granitic middle crust.

2. Geologic setting

The Hatagawa Shear Zone is one of a series of major

* Corresponding author. Tel.: +81-43-290-2857; fax: +81-43-290-2859.
E-mail address: kyu@earth.s.chiba-u.ac.jp (K. Kanagawa).

0191-8141/03/$ - see front matter © 2002 Elsevier Science Ltd. All rights reserved.
PII: S0191-8141(02)00048-2

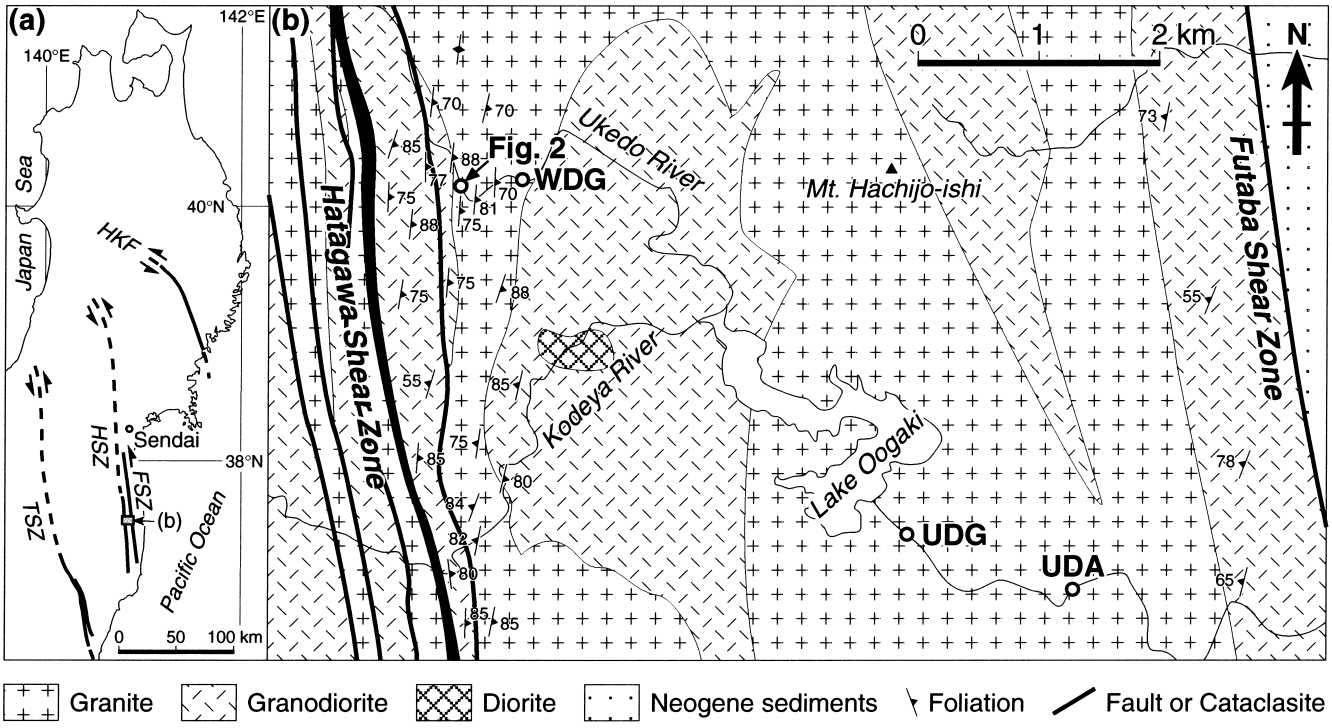

Fig. 1. (a) Index map showing major Cretaceous sinistral shear zones in NE Japan and the location of study area (b). *TSZ*: Tanakura Shear Zone, *HSZ*: Hatagawa Shear Zone, *FSZ*: Futaba Shear Zone, and *HKF*: Hizume–Kesen'numa Fault. (b) Geologic map of the study area compiled from Kubo et al. (1990) and Shigematsu and Yamagishi (2002), where three sample localities (UDA, UDG and WDG) and the location of Fig. 2 are shown.

NNW-trending sinistral shear zones in NE Japan (Fig. 1a) activated mainly during middle Cretaceous time (Otsuki and Ehiro, 1992). The age of ductile shearing and the total sinistral displacement along the shear zone have been estimated to be 106–86 Ma and ≈60 km, respectively (Otsuki and Ehiro, 1992). Quartz *c*-axis fabrics of Type I crossed girdle and *Y*-maximum patterns (Koshiya, 1988; Shigematsu and Yamagishi, 2002) suggest moderate temperatures during ductile shearing (e.g. Passchier and Trouw, 1996). In the study area the shear zone cuts through Early Cretaceous granitic rocks with K–Ar hornblende and biotite ages of 96–126 Ma (Kubo and Yamamoto, 1990), and is accompanied by a ≈50-m-thick cataclasite zone and subsidiary faults (Takagi et al., 2000; Shigematsu and Yamagishi, 2002; Fig. 1b). The shear zone extends up to 1.5 km in width on the east side of the cataclasite zone, where granitic rocks are regionally deformed and locally mylonitized with N-trending foliation oblique to the NNW-trend of the cataclasite zone and faults (Shigematsu and Yamagishi, 2002; Fig. 1b). In contrast, granitic rocks on the west side of the cataclasite zone are essentially undeformed except in sporadically developed NE-trending small-scale dextral shear zones (Shigematsu, 1999; Shigematsu and Tanaka, 2000; Takagi et al., 2000).

Progressive mylonitization of granite and aplite is well observed in the Hatagawa Shear Zone along the Ukedo River (Fig. 2). We follow the classification of mylonites after Sibson (1977). Aplite veins of 1–20 cm in width are preferentially mylonitized, although undeformed aplite veins are also present. Granite is strongly deformed there, and locally mylonitized in 1–3-m-wide zones adjacent to aplite veins. Deformed and mylonitized granite and aplite develop N-striking subvertical foliation with subhorizontal lineation (Fig. 2d). We collected six samples at two outcrops (Fig. 2a and b). Progressive mylonitization from strongly deformed granite through mylonite to ultramylonite is observed within a distance of ≈2 m at outcrop A, where a strongly deformed granite (SDG), a less deformed granite mylonite (GM1), a more deformed granite mylonite (GM2), and a granite ultramylonite (GUM) were collected (Fig. 2a). Mylonitization of two aplite veins ≈5 cm apart and the intervening granite is observed at outcrop B, where an aplite mylonite (AML) and an aplite ultramylonite (AUM) were collected (Fig. 2b). In both outcrops, granite mylonites occur in zones bounded by aplite veins, and their boundaries with the surrounding granite are sharp (Fig. 2a and b).

In addition to the above six samples, we also collected a weakly deformed granite (WDG) from the eastern margin of the Hatagawa Shear Zone, and an undeformed granite (UDG) and an undeformed aplite (UDA) outside the Shear Zone (Fig. 1b). All granite and aplite samples in this study have been collected from a single granite pluton with a K–Ar biotite age of 114 Ma (Kubo and Yamamoto, 1990; Kubo et al., 1990).

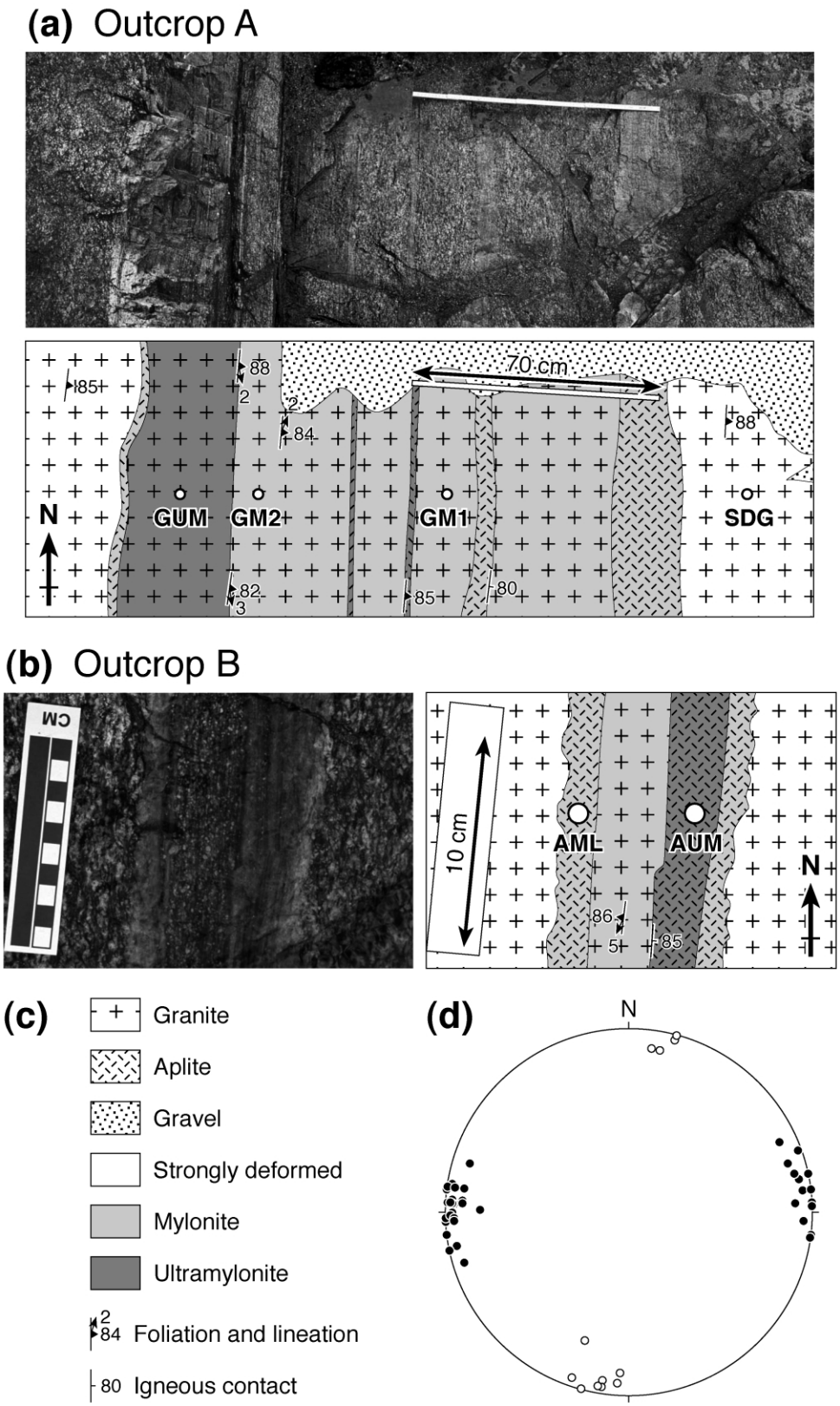

Fig. 2. (a) and (b) Photographs and sketches of the two mylonite outcrops, A and B, showing six sample localities (open circles). Outcrop B is located ≈100 m to NNW from outcrop A. (c) Keys to the sketches in (a) and (b). (d) Equal-area, lower hemisphere projections of lineation (open circles) and poles to foliation (closed circles) in an area including the two outcrops.

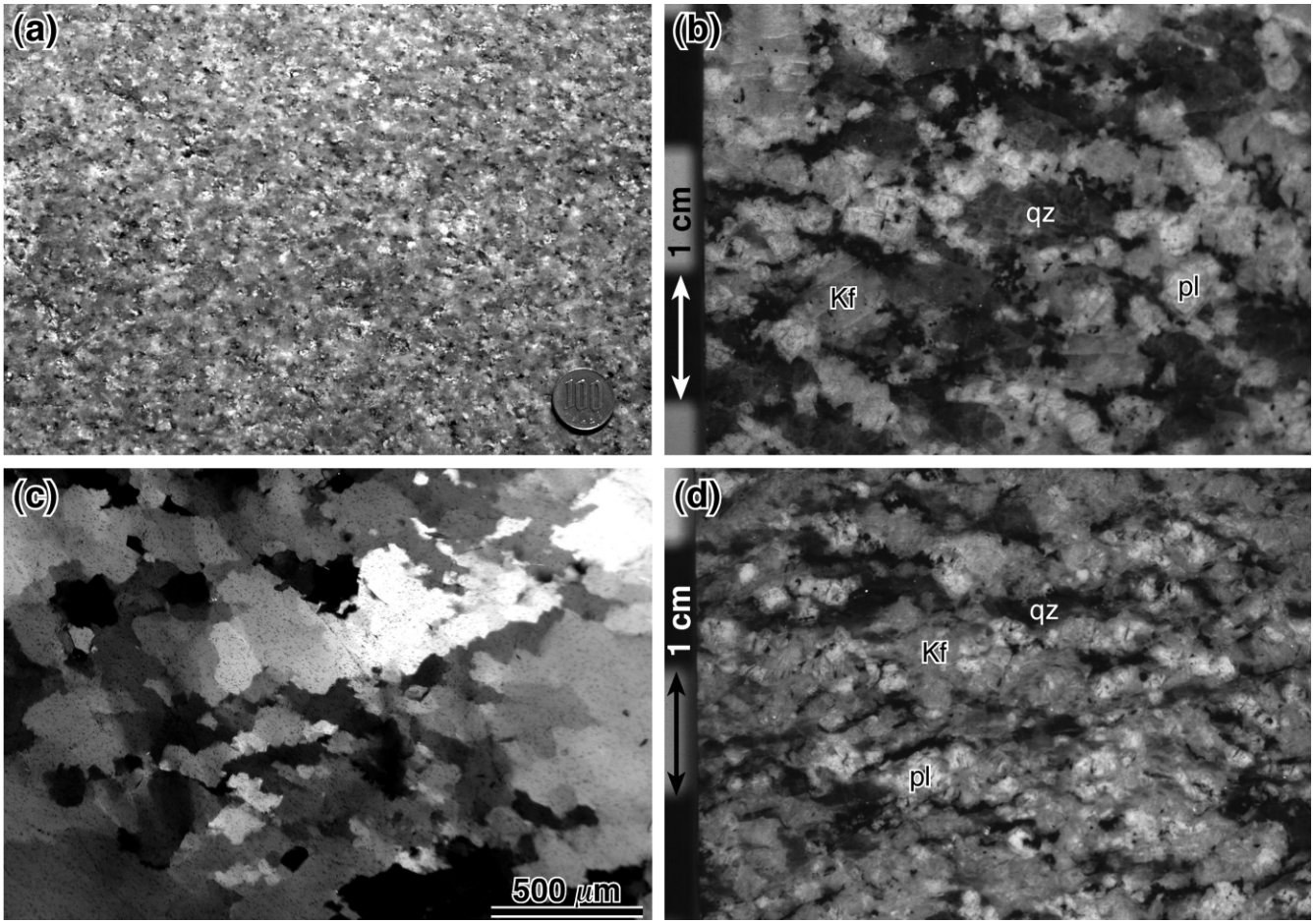

Fig. 3. Microstructures of non-mylonitic granite samples. (a) Outcrop surface of UDG. A coin at the bottom right is 2.2 cm in diameter. (b) Polished specimen surface of WDG. (c) Optical micrograph in CPL (crossed polarized light) of quartz aggregate in WDG. (d) Polished specimen surface of SDG. qz: quartz, pl: plagioclase, and Kf: K-feldspar.

3. Microstructures

Optical and back-scattered electron (BSE) microstructures of the collected samples were observed viewing downward in subhorizontal *XZ* sections cut perpendicular to the foliation (*XY*) and parallel to the lineation (*X*). Undeformed granite and aplite samples without a foliation or lineation are cut parallel to the average orientation of the other samples' *XZ* sections. Foliation trace and lineation are horizontal in all the micrographs shown in Figs. 3–7, except for Fig. 6e and f, where they are vertical.

3.1. Non-mylonitic granite samples (UDG, WDG and SDG)

Sample UDG has an isotropic fabric (Fig. 3a). Quartz grains do not show any sign of intracrystalline deformation, and their grain size (530 ± 470 μm) is as coarse as that of euhedral plagioclase grains. In sample WDG, quartz aggregates are elongate (Fig. 3b). Quartz grains have relatively small grain sizes (220 ± 210 μm), locally developed subgrains, and serrated grain boundaries due to dynamic recrystallization and grain boundary migration (e.g. Fig. 3c). Quartz aggregates in sample SDG are more elongate in shape than those in WDG, and are deflected around feldspar grains (Fig. 3d). Quartz grains of SDG are much smaller in grain size (70 ± 60 μm) than those of WDG.

3.2. Less deformed granite mylonite sample (GM1)

Sample GM1 exhibits a porphyroclast-in-matrix microstructure (Fig. 4a), containing abundant porphyroclasts (200–1400 μm in size) of plagioclase and K-feldspar in either a monomineralic matrix of quartz, K-feldspar and biotite, or a fine-grained (≤50 μm) polymineralic matrix made up of plagioclase, K-feldspar, quartz and biotite (Fig. 4a–c and f). Elongated monomineralic quartz aggregates form ribbons (Fig. 4e), while fine-grained polymineralic aggregates form layers (Fig. 4f). Quartz ribbons and layers of fine-grained polymineralic aggregate are dominant in the matrix, and characterize the mylonitic foliation (Fig. 4a–c). Orientations of elongate K-feldspar porphyroclasts (*S*), oblique alignment of elongate recrystallized grains in quartz ribbons (S'), quartz ribbons and layers of fine-grained

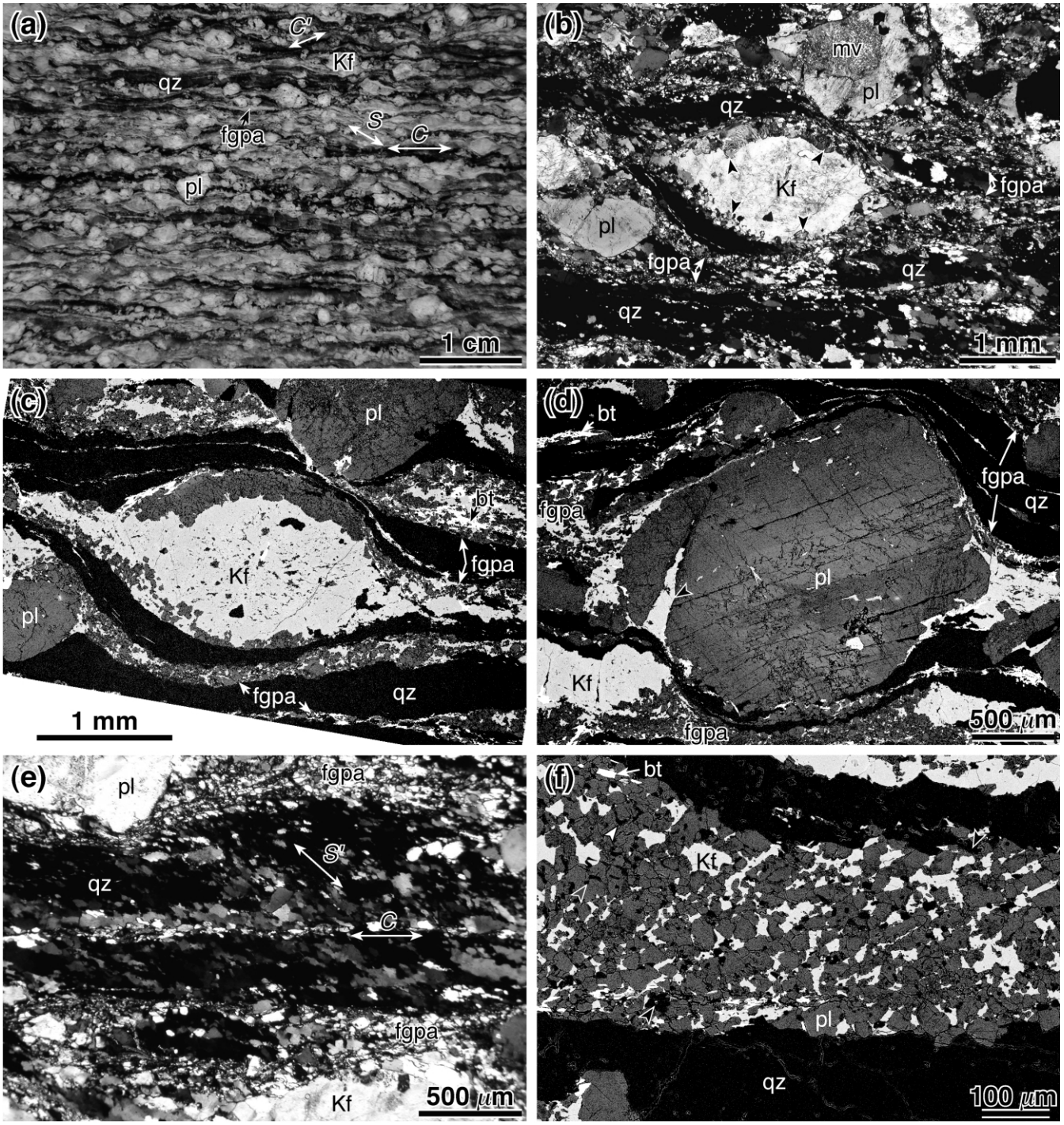

Fig. 4. Microstructures of GM1. (a) Polished specimen surface. (b) Optical micrograph (CPL). (c) BSE (backscattered electron) micrograph of a central area of (b). (d) BSE micrograph of a plagioclase porphyroclast (center). (e) Optical micrograph of quartz ribbons (CPL). (f) BSE micrograph of fine-grained polymineralic aggregate of plagioclase, K-feldspar, quartz and biotite. S, S', C and C': planar fabrics described in text, bt: biotite, mv: muscovite, and fgpa: fine-grained polymineralic aggregate. Other mineral abbreviations are the same as in Fig. 3.

polymineralic aggregate (C), and shear bands (C') (white arrows in Fig. 4a and e) all indicate a sinistral sense of shear.

Myrmekite lobes are well developed around K-feldspar porphyroclasts along their boundaries subparallel to the mylonitic foliation (black arrowheads in Fig. 4b, see also Fig. 4c). Plagioclase porphyroclasts are locally fractured (e.g. black arrowhead in Fig. 4d), and their fractures as well as pressure shadows are commonly filled with K-feldspar (Fig. 4d). Porphyroclast plagioclase is locally replaced by a fine-grained aggregate of muscovite (e.g. mv in Fig. 4b). Recrystallized grains and subgrains in quartz ribbons are elongate, with their alignment defining oblique foliation

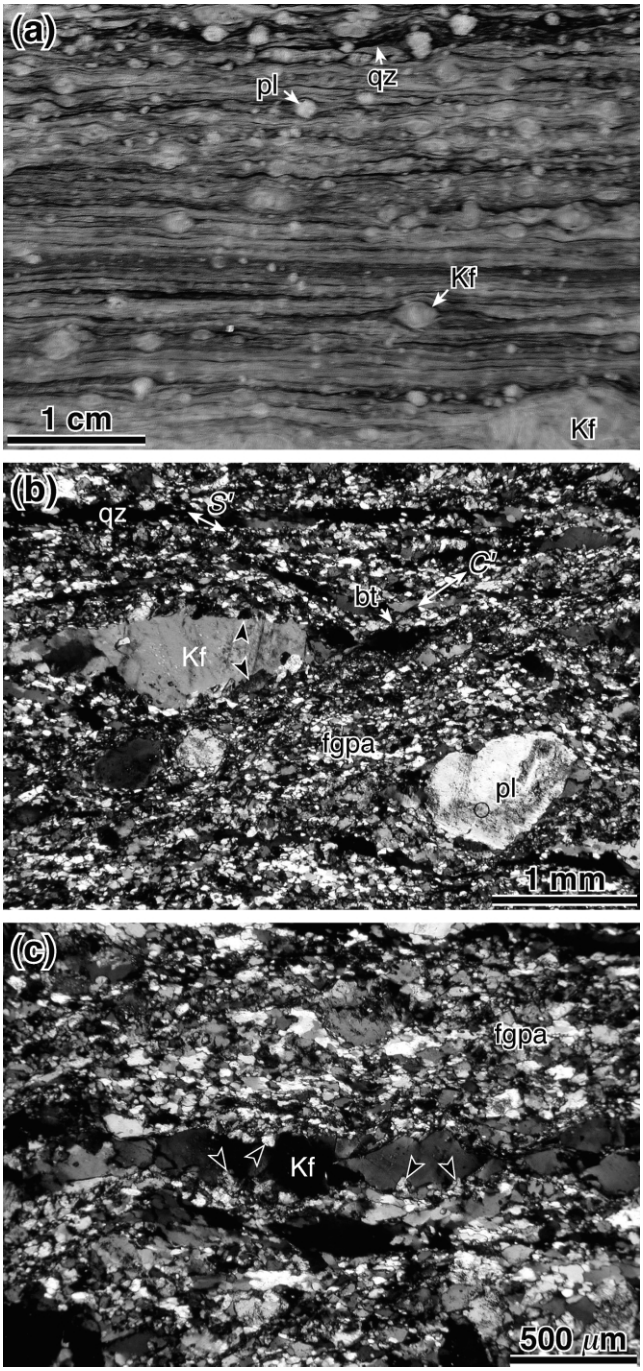

Fig. 5. Microstructures of GM2. (a) Polished specimen surface. (b) Optical micrograph (CPL). (c) Optical micrograph (CPL) showing a boudinaged K-feldspar ribbon (center). Mineral and other abbreviations are the same as in Figs. 3 and 4.

(e.g. S' in Fig. 4e). Many grains in quartz ribbons display their *c*-axes oriented approximately normal to the *XZ* section (i.e. in the *Y*-direction; Fig. 4e), as described later. Plagioclase is dominant, and K-feldspar is interstitial in the fine-grained polymineralic aggregates (Fig. 4f). Quartz occurs as vermicular or globular inclusions (typically ≤ 10 μm in size) in plagioclase (e.g. white and gray arrowheads, respectively, in Fig. 4f), or as relatively coarse (>10 μm) isolated grains (e.g. black arrowheads in Fig. 4f).

3.3. More deformed granite mylonite sample (GM2)

In sample GM2, feldspar porphyroclasts form a smaller volume fraction, and are smaller in size than those in GM1 (Fig. 5a), while fine-grained polymineralic aggregates are dominant in the matrix (Fig. 5b and c). Quartz ribbons and layers of fine-grained polymineralic aggregate define a mylonitic foliation (Fig. 5a). Asymmetric microstructures indicative of shear sense are rarely found at the specimen scale (Fig. 5a), although orientations of oblique grain shape foliation (S') in quartz ribbons and shear bands (C') relative to mylonitic foliation found on thin section scale (white arrows in Fig. 5b) indicate a sinistral sense of shear.

Monomineralic K-feldspar aggregates are commonly elongate parallel to the mylonitic foliation, forming K-feldspar ribbons (Fig. 5c). They exhibit pinch-and-swell structures with undulatory extinction in neck areas (Fig. 5c). Myrmekite lobes are well developed not only along K-feldspar porphyroclast boundaries subparallel to mylonitic foliation, but also along K-feldspar ribbon boundaries (black arrowheads in Fig. 5b and c).

3.4. Granite ultramylonite sample (GUM)

Sample GUM contains a few feldspar porphyroclasts (Fig. 6a), and is largely composed of a fine-grained polymineralic aggregate, which is a homogeneous mixture of plagioclase, K-feldspar, quartz and biotite (Fig. 6b–d). Rare asymmetric mantled porphyroclasts (black arrowhead in Fig. 6a) indicate a sinistral sense of shear. Myrmekite lobes are well developed around K-feldspar porphyroclasts (black arrowheads in Fig. 6b and c). Relatively coarse (>10 μm) quartz grains in contact with both plagioclase and K-feldspar grains are more abundant in the fine-grained polymineralic aggregate than those in GM1 (Fig. 6d), although vermicular or globular quartz inclusions in plagioclase (e.g. white and black arrowheads in Fig. 6d) are as common as those in GM1. GUM also contains rare garnet grains (Fig. 6b), some of which exhibit optical zoning with a pinkish core and colorless rim (cf. Fig. 7d).

K-feldspar porphyroclasts show that, relative to core regions, Na concentration decreases while K concentration increases in porphyroclast rims adjacent to myrmekite lobes (e.g. black arrowheads in Fig. 6e and f). Myrmekite lobes growing toward interiors of K-feldspar porphyroclasts locally leave isolated or almost isolated K-feldspar porphyroclast rims behind (e.g. gray arrowheads in Fig. 6e and f). K-feldspar grains in fine-grained polymineralic aggregate (e.g. white arrowheads in Fig. 6e and f) are as poor in Na concentration and as rich in K concentration as K-feldspar in porphyroclast rims adjacent to myrmekite lobes.

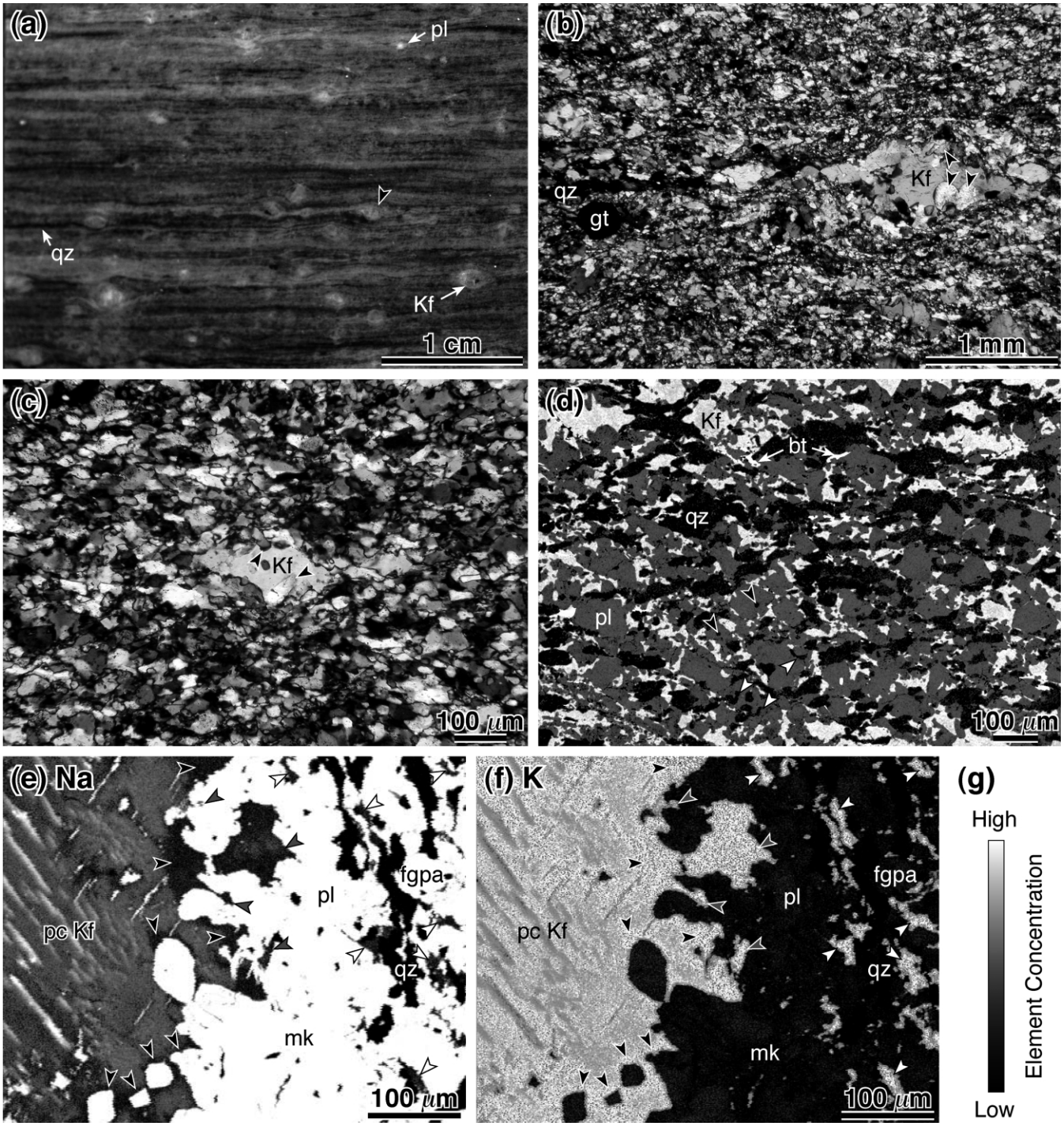

Fig. 6. Microstructures of GUM. (a) Polished specimen surface. (b) Optical micrograph (CPL). (c) Optical micrograph (CPL) showing a close-up view of fine-grained polymineralic aggregate. (d) BSE micrograph of fine-grained polymineralic aggregate. (e) and (f) Distributions of Na (e) and K (f) concentrations in an area within and adjacent to a K-feldspar porphyroclast. The porphyroclast, myrmekite aggregate and fine-grained polymineralic aggregate occupy the left, central and right parts of the area, respectively. (g) Gray scale for element concentration in (e) and (f). gt: garnet, mk: myrmekite, and pc Kf: porphyroclast K-feldspar. Other mineral abbreviations are the same as in Figs. 3 and 4.

3.5. Aplite samples (UDA, AML and AUM)

Microstructures of aplite samples are essentially the same as in their granite counterparts. All aplite samples contain small amounts of garnet (Fig. 7b–d). Optically zoned garnet grains with pinkish cores and colorless rims are common in samples AML and AUM (e.g. Fig. 7d). Grains within the fine-grained polymineralic matrix anastomose around the garnet grains (Fig. 7d). Sample UDA has no features indicating intracrystalline deformation (Fig. 7a).

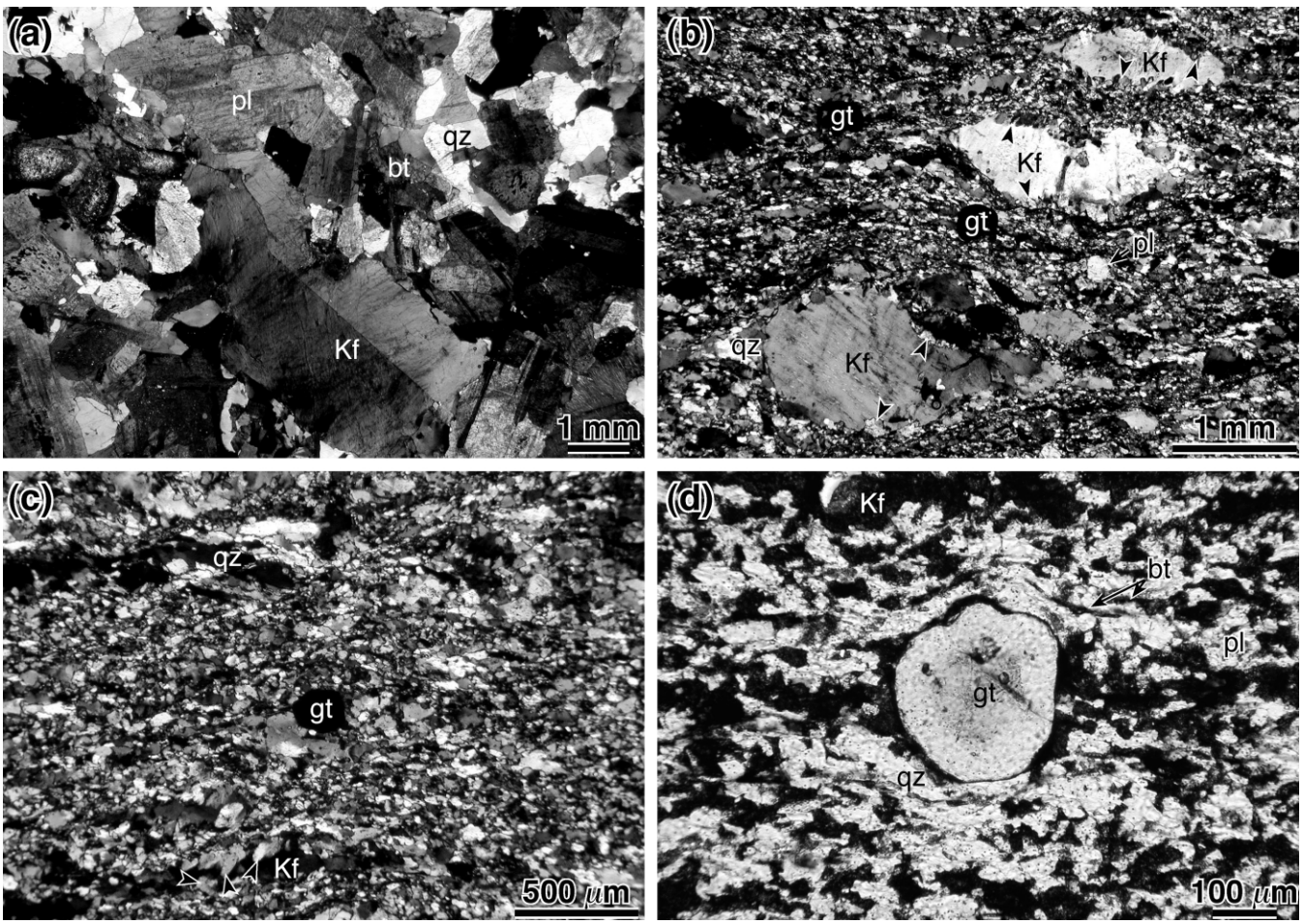

Fig. 7. Optical microstructures of aplite samples. (a), (b) and (c) are in CPL, while (d) is in PPL (plane-polarized light). (a) UDA. (b) AML. (c) AUM. (d) A zoned garnet grain (center) in AUM. K-feldspar in (d) is stained for modal analysis. Mineral abbreviations are the same as in Figs. 3, 4 and 6.

Sample AML exhibits a porphyroclast-in-matrix microstructure with the matrix largely composed of fine-grained polymineralic aggregate (Fig. 7b). Myrmekite lobes are developed along K-feldspar porphyroclast boundaries subparallel to the mylonitic foliation (black arrowheads in Fig. 7b). Sample AUM is mostly composed of fine-grained polymineralic aggregate (Fig. 7c). K-feldspar locally occurs as ribbons (Fig. 7c) with myrmekite lobes along their boundaries (black arrowheads in Fig. 7c).

4. Modal compositions[1]

Modal compositions were determined by point counting with a traverse spacing of 300 μm for each sample using stained thin sections (e.g. Fig. 7d); 2000 point counts were recorded for each section. Major constituent minerals in different microstructural units such as porphyroclast, monomineralic aggregate, fine-grained polymineralic aggregate and myrmekite were counted separately.

The granite and aplite samples contain 24–41 mode% quartz, 26–41 mode% plagioclase, 21–47 mode% K-feldspar, and 1–10 mode% biotite (Fig. 8a). Besides these minerals, sample GUM and the aplite samples contain 0.3–0.6 mode% garnet (Fig. 8a). The changes in bulk modal composition are not systematic in the non-mylonitic granites, while a significant increase in K-feldspar content and a decrease in content of quartz, plagioclase and biotite are observed with increasing mylonitization in the granite mylonites (Fig. 8a). The modal composition of GUM is thus close to those of the aplites (Fig. 8a). The changes in modal composition are rather minor in the aplites compared with those in the granite mylonites (Fig. 8a).

A major difference in modal composition between the non-mylonites and mylonites is an almost absence in the non-mylonites of fine-grained polymineralic aggregate and monomineralic K-feldspar aggregate occurring in ribbons, fracture fillings and pressure shadows (Fig. 8b). The total modal content of plagioclase and K-feldspar porphyroclasts decreases with increasing mylonitization from 35.9% (GM1) to 7.1% (GUM) in the granite mylonites, and from

[1] Tables containing data are available as a compressed BinHex-format Microsoft® Excel file "THK(JSG)Tables.sit.hqx" at ftp://ftp-es.s.chiba-u.ac.jp/pub/struct.

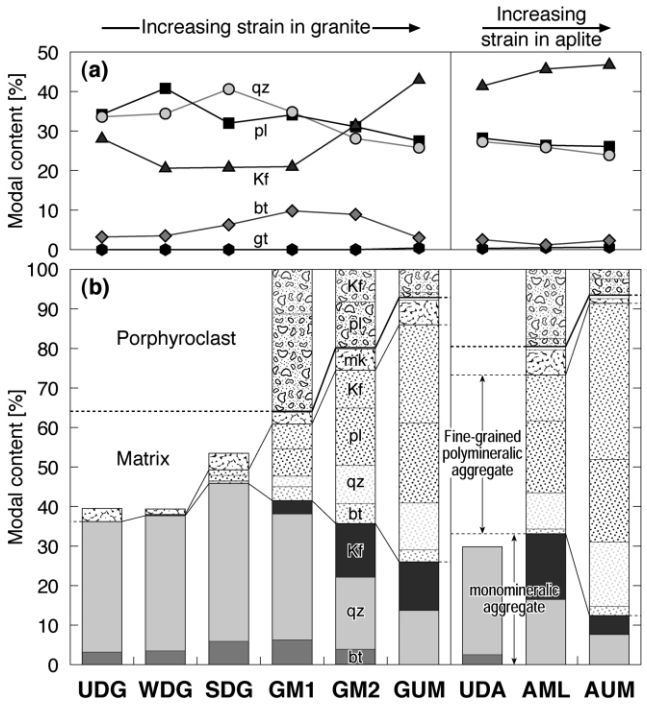

Fig. 8. Modal compositions of the studied samples. (a) Bulk modal compositions of major constituent minerals. (b) Modal compositions of major constituent minerals in different microstructural units. qz: quartz, pl: plagioclase, Kf: K-feldspar, bt: biotite, gt: garnet, mk: myrmekite.

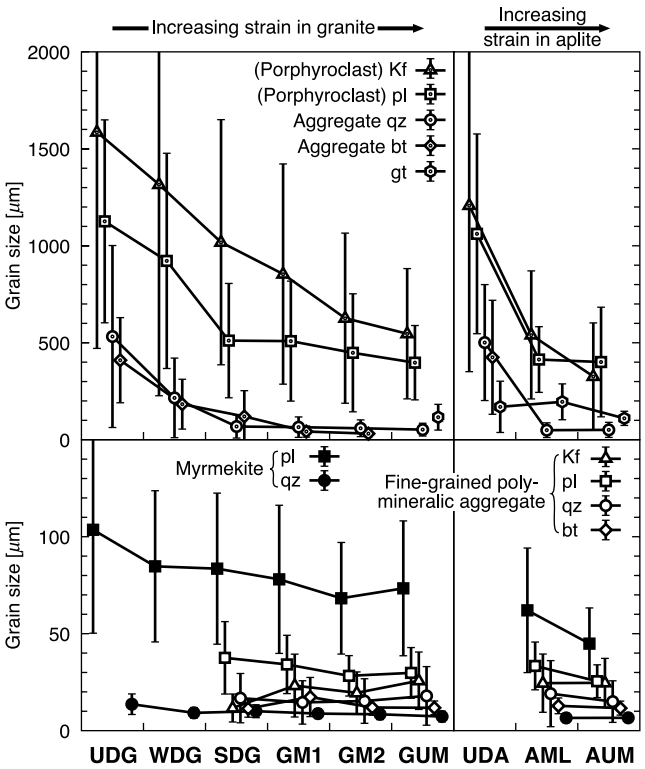

Fig. 9. Grain-size variations of major constituent minerals in the studied samples. Mineral abbreviations are the same as in Fig. 8. Symbols with vertical bars represent average grain sizes and their standard deviations.

19.5% (AML) to 6.5% (AUM) in the aplite mylonites (Fig. 8b). The modal content of quartz, biotite and K-feldspar aggregates also decreases with increasing mylonitization, except for that of K-feldspar increasing from GM1 to GM2 (Fig. 8b). In contrast, the modal content of fine-grained polymineralic aggregate increases with increasing mylonitization from 19.4% (GM1) to 60% (GUM) in the granite mylonites, and from 40.2% (AML) to 79% (AUM) in the aplite mylonites (Fig. 8b). Quartz, plagioclase and K-feldspar in the fine-grained polymineralic aggregate increase in modal content with increasing mylonitization (Fig. 8b).

5. Grain-size variations[1]

In each sample, grain boundaries of 38–1354 (mostly 100–400) grains of every major constituent mineral in different microstructural units were traced from a number of optical micrographs. Grain diameters of individual grains were then obtained by image analysis as diameters of circles having equal areas with those of grain areas, and their averages and standard deviations were calculated. Corrections taking account of sectioning effects have not been made.

Grain-size reduction of major constituent minerals in porphyroclast and monomineralic aggregate is clearly observed with increasing deformation and mylonitization, although the changes in grain size other than porphyroclast K-feldspar are minor in the mylonites (Fig. 9). Garnet does not show any significant change in grain size (Fig. 9). The grain size of myrmekite plagioclase slightly decreases with increasing deformation and mylonitization, while myrmekite quartz has almost constant grain size of 7–10 ± 3 μm (Fig. 9).

Constituent minerals in fine-grained polymineralic aggregates are mostly smaller than 50 μm, and do not show significant changes in grain size with increasing mylonitization (Fig. 9). The grain size of plagioclase slightly decreases, whereas that of K-feldspar slightly increases (Fig. 9). Quartz grains in fine-grained polymineralic aggregates have a bimodal grain-size distribution with a smaller sharp peak at ≤10 μm and a larger broad peak around 20–30 μm (Fig. 10).

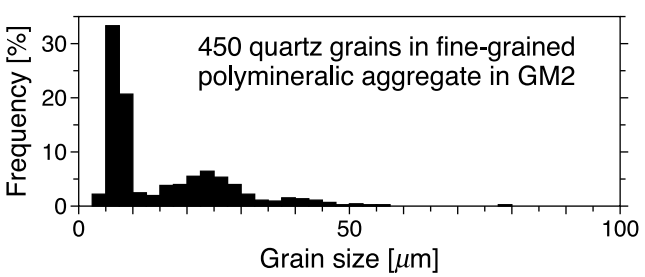

Fig. 10. Grain-size distribution of 450 quartz grains in fine-grained polymineralic aggregate of GM2.

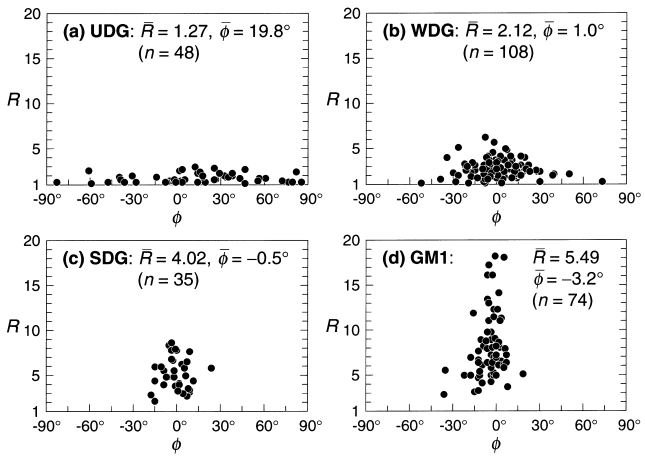

Fig. 11. Aspect ratio (R)–long-axis orientation (ϕ) diagrams of quartz aggregates on XZ sections of four granite samples. ϕ is measured anticlockwise from the macroscopic foliation trace. $\bar{R}$ and $\bar{\phi}$ denote the aspect ratio and long-axis orientation, respectively, of the averaged shape of quartz aggregates. n: number of quartz aggregates measured.

6. Quartz aggregate shapes[1]

Aspect ratios and long-axis orientations of individual quartz aggregates in four granite samples, UDG, WDG, SDG and GM1, were measured in order to obtain information on finite strain. Because individual grains in quartz aggregates are dynamically recrystallized, it is highly unlikely that they preserve information on finite strain. However, individual quartz aggregates may give at least a crude measure of finite strain. Outlines of 35–108 quartz aggregates were traced from polished XZ-section slabs. Aspect ratios (R) and long-axis orientations (ϕ) with respect to macroscopic foliation trace, of individual quartz aggregates were then obtained by image analysis as axial ratios and long-axis orientations of the best-fit ellipses, and their averages ($\bar{R}$ and $\bar{\phi}$) were calculated from the averaged ellipse shape tensor (Wheeler, 1984).

Quartz aggregates in UDG have small aspect ratios ($R \leq 3.0$) and quasi-random orientations (Fig. 11a). With increasing deformation, quartz aggregates become more elongated, and their long-axis orientations become more concentrated around the orientation of foliation (Fig. 11b–d). The average aspect ratio ($\bar{R}$) increases with increasing deformation from 1.27 (UDG) to 5.49 (GM1) (Fig. 11), while the average long-axis orientation ($\bar{\phi}$) remains close to 0°.

7. Quartz c-axis fabrics[1]

c-Axis orientations of over 200 quartz grains in monomineralic quartz aggregates were measured for four granite samples, SDG, GM1, GM2 and GUM, using an optical microscope equipped with a universal stage.

The quartz c-axis fabric of non-mylonitic SDG exhibits a single maximum in the Y-direction (Fig. 12a). The quartz c-axis fabric of GM1 is characterized by two maxima located 20–30° away from the Y-axis toward the Z-axis, and a subsidiary maximum at the periphery of the diagram ≈30° anticlockwise away from the Z-axis (Fig. 12b). The quartz c-axis fabrics of GM2 and GUM are characterized by asymmetric, Type I crossed girdles (Lister, 1977) with poorly developed trailing legs, having three maxima located at approximately the same positions as those in GM1 (Fig. 12c and d). The quartz c-axis fabric of GUM is close to a

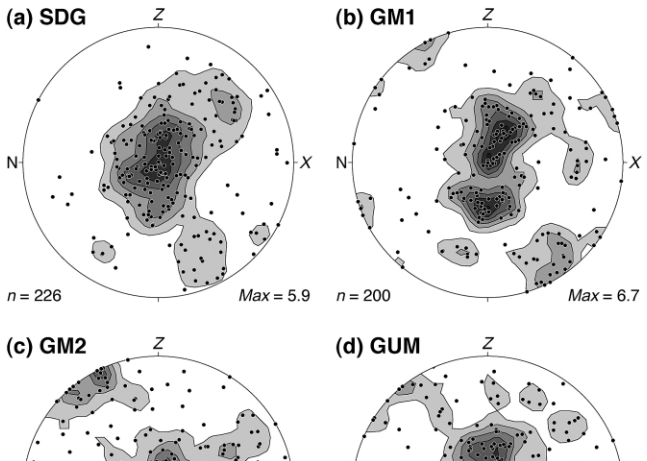

Fig. 12. Quartz c-axis fabrics in quartz aggregates of four granite samples. Equal-area, lower hemisphere projections using Neil Mancktelow's *StereoPlot*. Contoured at multiples of uniform distribution. n: number of grains measured, *Max*: maximum density normalized by uniform distribution, and N: approximate direction of north.

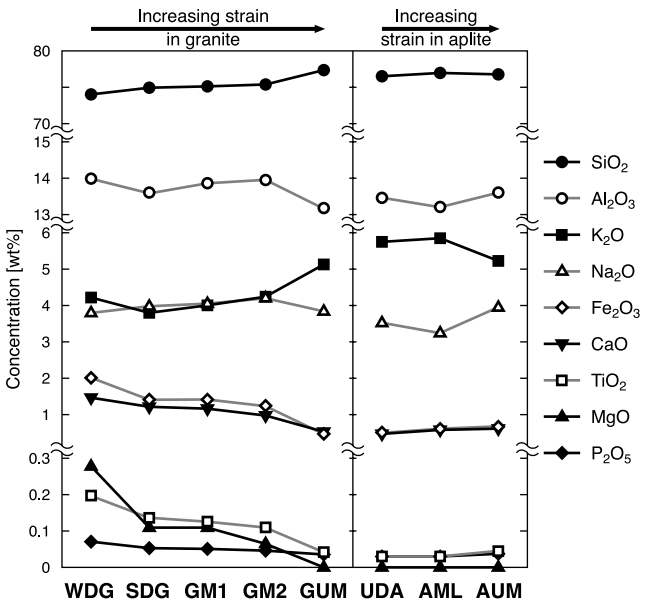

Fig. 13. Bulk chemical compositions of the studied samples.

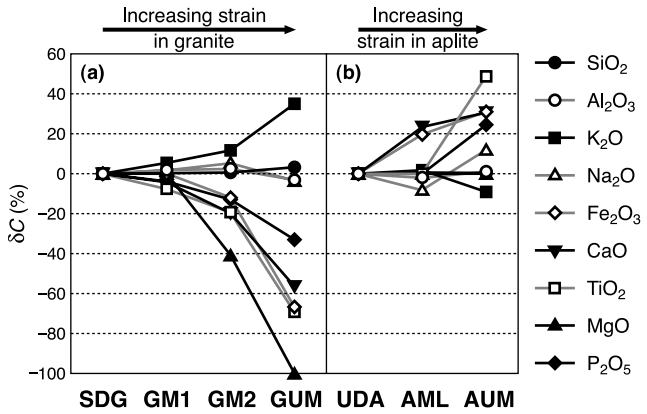

Fig. 14. Changes in major element concentration (δC) relative to SDG in granite samples at outcrop A (a) and those relative to UDA in aplite samples (b).

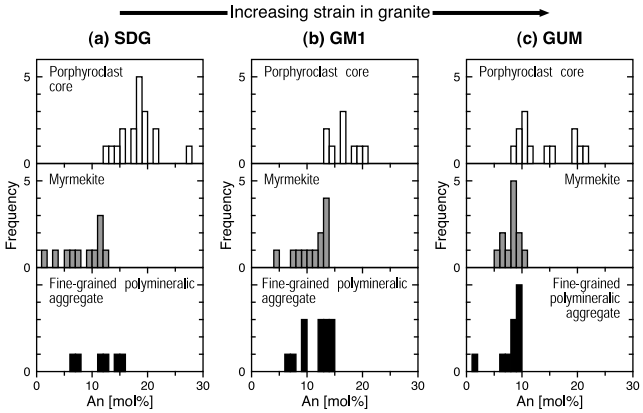

Fig. 15. Anorthite components of plagioclase in porphyroclast core, myrmekite and fine-grained polymineralic aggregate of three granite samples.

single girdle (Fig. 12d). The leading edges of asymmetric Type I crossed girdles of GM2 and GUM oriented anticlockwise away from the *Z*-axis (Fig. 12c and d) indicate a sinistral sense of shear, as indicated by the previously described microstructural shear-sense indicators.

8. Bulk chemical compositions[1]

Bulk chemical compositions of the samples except for UDG were determined by X-ray fluorescence (XRF) spectroscopy using a Philips PW1480 at the Department of Geology, University of Tokyo, following the sample preparation and analytical procedures described by Yoshida and Takahashi (1997).

With increasing deformation and mylonitization of the granite, an overall increase in K_2O, and a decrease in CaO, Fe_2O_3, MgO, TiO_2 and P_2O_5 is observed (Figs. 13 and 14a). In addition, sample GUM is slightly richer in SiO_2 and poorer in Al_2O_3 than the other granite samples (Figs. 13 and 14a). Thus the bulk chemical composition of GUM is similar to those of aplites in being rich in SiO_2 and K_2O, poor in CaO, Fe_2O_3 and TiO_2, and absent in MgO (Fig. 13).

Although no systematic change in bulk chemical composition is apparent with increasing mylonitization of the aplite (Fig. 13), changes in element concentration relative to sample UDA reveal a systematic increase in CaO, Fe_2O_3, TiO_2 and P_2O_5 (Fig. 14b) and a decrease in K_2O, which are opposite to changes in the granites (Fig. 14a).

9. Chemical compositions of feldspars and garnet[1]

Chemical compositions of plagioclase and K-feldspar in three granite samples, SDG, GM1 and GUM, and those of zoned garnet in AUM were determined by electron microprobe analysis (EPMA) using a JEOL JXA8900 at the Chemical Analysis Center, Chiba University, and a JEOL JXA8900L at the Department of Geology, University of Tokyo.

Porphyroclast-core plagioclase is mostly An_{9-20} (Fig. 15). The chemical composition of myrmekite plagioclase is distinctly different from that of porphyroclast-core plagioclase (Fig. 15). The former (mostly An_{5-14}) is more albitic than the latter in all three samples, and similar to that of plagioclase in the fine-grained polymineralic aggregate (An_{6-15}) (Fig. 15).

The chemical composition of porphyroclast-core K-feldspar varies from Or_{82} to Or_{97} (Fig. 16). In contrast, the chemical composition of K-feldspar in fine-grained polymineralic aggregate is concentrated around Or_{95-97} (Fig. 16). The fine-grained K-feldspar tends to be richer in the orthoclase component than the porphyroclast-core K-feldspar (Fig. 16).

As described above, optically zoned garnet grains with pinkish cores and colorless rims are common in samples GUM, AML and AUM. Compositional profiles across such zoned garnet grains in AUM reveal an increase in Ca concentration and a decrease in Fe and Mg concentrations at their rims (e.g. Fig. 17), indicating that colorless rims of zoned garnet grains are rich in grossular component.

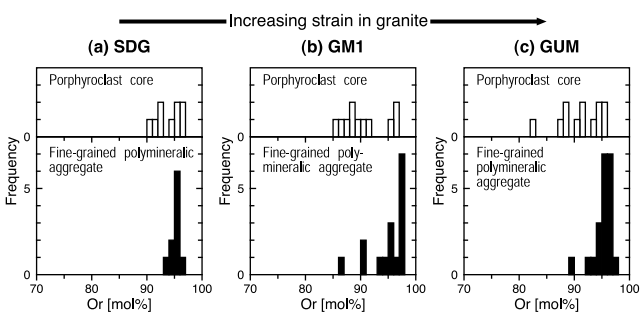

Fig. 16. Orthoclase components of K-feldspar in porphyroclast core and fine-grained polymineralic aggregate of three granite samples.

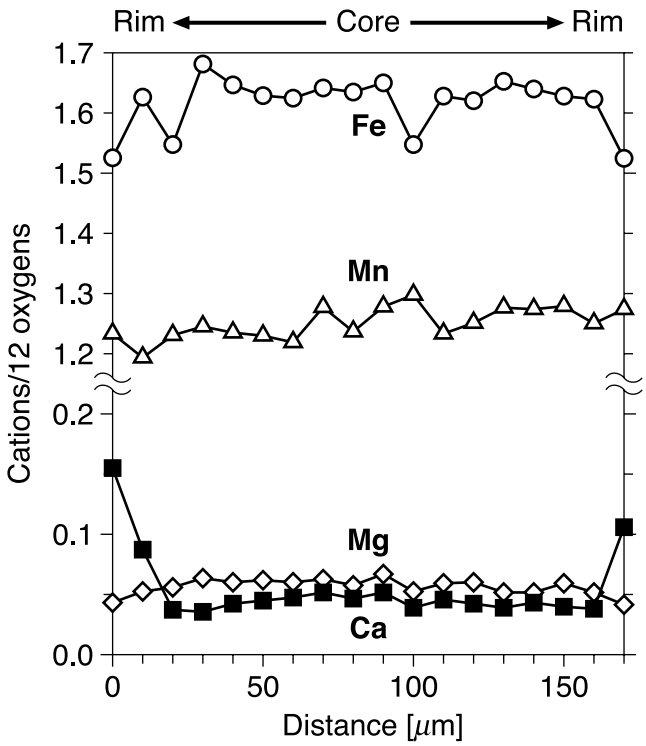

Fig. 17. Fe, Mn, Mg and Ca concentration profiles across a garnet grain in AUM.

10. Discussion

10.1. Strain variations

Assuming homogeneous deformation of initial randomly oriented individual quartz aggregates, we can estimate two-dimensional finite strains recorded by the quartz aggregates from their averaged ellipse shape tensors (Shimamoto and Ikeda, 1976; Wheeler, 1984). The estimated finite strain ratio in *XZ* sections gradually increases from 1.27 in UDG, through 2.12 in WDG and 4.02 in SDG, to 5.49 in GM1 (Fig. 11), indicating high strains accumulated in the granite mylonites. It must further increase toward the ultramylonite, although data have not been obtained due to difficulty in tracing outlines of quartz aggregates in both samples GM2 and GUM. Assuming simple shear deformation such that the *Y*-axis is parallel to shear plane and perpendicular to the shear direction, the equivalent shear strains are 0.24 in UDG, 0.77 in WDG, 1.51 in SDG, 1.92 in GM1, and must be much larger in GM2 and GUM. Thus strain is localized in narrow (1 cm–3 m) zones of mylonite along the Hatagawa Shear Zone. Shear strains larger than 1.9 are comparable with those in other granite mylonites (e.g. Berthé et al., 1979; Vauchez, 1987; Fliervoet et al., 1997).

10.2. Progressive mylonitization

Deformation of the non-mylonitic granites is represented by elongation of quartz aggregates (Fig. 3b and d) due to crystal plastic deformation of quartz, and grain-size reduction of constituent minerals such as quartz, plagioclase, K-feldspar and biotite (Fig. 9). Grain-size reduction of aggregate quartz (Fig. 9) is due to dynamic recrystallization (e.g. Fig. 3c), while that of biotite may be due to comminution associated with slip along basal planes.

Mylonitization of the granite and aplite involves a decrease in modal content and grain size of plagioclase and K-feldspar porphyroclasts, a decrease in modal content of aggregate quartz and biotite, an appearance of K-feldspar aggregate in ribbons, fracture fillings and pressure shadows, and an increase in modal content of fine-grained polymineralic aggregate (Figs. 8b and 9). Grain-size reduction of porphyroclast plagioclase proceeds mainly by fracturing (e.g. Fig. 4d), while that of porphyroclast K-feldspar proceeds as myrmekite lobes grow toward the porphyroclast interior (e.g. Figs. 4b and c, 5b, 6b and 7b). The decrease in modal content of porphyroclast plagioclase may be partly due to its incorporation into fine-grained polymineralic aggregate, and partly to its replacement by muscovite (e.g. Fig. 4b). In contrast, the decrease of porphyroclast K-feldspar is not only due to its replacement by myrmekite, but also to its elongation into ribbons (e.g. Figs. 5c and 7c) by crystal plasticity, as indicated by undulatory extinction in the neck regions of boudinaged ribbons. The decrease in modal content of aggregate quartz and biotite is attributable to their incorporation into fine-grained polymineralic aggregates. K-feldspar aggregates are formed by elongation of porphyroclasts into ribbons as well as by K-feldspar filling of fractures and pressure shadows (e.g. Fig. 4d). The latter may be precipitated from solution, as discussed later.

Fine-grained (≤ 10 μm) polymineralic aggregates made up of plagioclase + K-feldspar + quartz ± biotite in a mylonite matrix have also been described in a quartz–feldspar mylonite from the Cucamonga fault zone in southern California (Behrmann and Mainprice, 1987), and in quartzo-feldspathic ultramylonites from the Redbank Deformed Zone in central Australia (Fliervoet et al., 1997). Although the fine-grained polymineralic aggregate has been inferred to have formed through chemical reactions in both cases, the reactions have not been specified (Behrmann and Mainprice, 1987; Fliervoet et al., 1997). The fine-grained polymineralic aggregate in the granite and aplite mylonites along the Hatagawa Shear Zone is derived mainly from the products of myrmekite-forming reaction, as discussed below.

Most plagioclase grains in fine-grained polymineralic aggregate are thought to be derived from the myrmekite plagioclase, because they contain vermicular or globular quartz inclusions (e.g. Figs. 4f and 6d), and also because they have chemical compositions (An_{6-15}) similar to those of myrmekite plagioclase (An_{5-14}) but distinctly different from porphyroclast-core plagioclase (An_{9-20}) (Fig. 15). Interstitial K-feldspar grains in fine-grained polymineralic aggregate (e.g. Figs. 4f and 6d) likely originate from isolated porphyroclast rims between myrmekite lobes

growing toward the interiors of porphyroclasts (e.g. gray arrowheads in Fig. 6e and f). This is supported by the chemical composition of K-feldspar in fine-grained polymineralic aggregates, which is similar to that in porphyroclast rims adjacent to myrmekite lobes (e.g. black and white arrowheads in Fig. 6e and f), but different from that of porphyroclast-core K-feldspar (Fig. 16). Like fracture-filling and pressure-shadow K-feldspar, interstitial K-feldspar may also be precipitated from solution. In both granite and aplite mylonites, the grain size of K-feldspar in fine-grained polymineralic aggregate slightly increases with increasing mylonitization (Fig. 9), and the modal content of monomineralic K-feldspar aggregate decreases in the granite and aplite ultramylonites (Fig. 8b). These observations suggest that the K-feldspar aggregates are also incorporated into the fine-grained polymineralic aggregate with increasing mylonitization.

A smaller sharp peak at <10 μm in grain-size distribution of quartz grains in fine-grained polymineralic aggregate (Fig. 10) corresponds well to the grain size of myrmekite quartz ($7-10 \pm 3$ μm; Fig. 9), supporting the suggestion that vermicular or globular quartz inclusions in plagioclase of the fine-grained polymineralic aggregate (Figs. 4f and 6d) are derived from the myrmekite quartz. Another broad peak at 20–30 μm (Fig. 10) represents relatively coarse isolated quartz grains in the fine-grained polymineralic aggregate (Figs. 4f and 6d). Because quartz grains are locally being stripped off from quartz ribbons into fine-grained polymineralic aggregate (e.g. a black arrowhead at the top right in Fig. 4f), isolated quartz grains are likely derived from quartz ribbons, although they are smaller than the grain size of ribbon quartz (50–60 μm on average; Fig. 9).

Thus the fine-grained polymineralic aggregate is likely formed by mixing of myrmekite lobes and their interstitial K-feldspar isolated from porphyroclast rims and/or precipitated from solution, with minor amounts of quartz, biotite and K-feldspar grains incorporated from their monomineralic aggregate. Increasing amounts of fine-grained polymineralic aggregate with increasing mylonitization therefore implies that the myrmekite-forming reaction proceeded with mylonitization of the granite and aplite along the Hatagawa Shear Zone.

10.3. Myrmekite-forming reaction

The myrmekite-forming reaction plays a key role in the development of the granite and aplite mylonites along the Hatagawa Shear Zone, as discussed above. The occurrence of myrmekite lobes along K-feldspar porphyroclast boundaries subparallel to mylonitic foliation (Figs. 4b and c, 5b, 6b and 7b), which are similar to those reported by Simpson (1985) and Simpson and Wintsch (1989), also indicate an intimate relationship between deformation and the myrmekite-forming reaction.

Simpson and Wintsch (1989) proposed a deformation-induced K-feldspar replacement by myrmekite in granitic mylonites as follows:

$$\underset{\text{porphyroclast K-feldspar}}{(1+x)KAlSi_3O_8} + (1-x)Na^+ + xCa^{2+} \rightarrow \underset{\text{myrmekite plagioclase}}{Na_{1-x}Ca_xAl_{1+x}Si_{3-x}O_8} + \underset{\text{myrmekite quartz}}{4xSiO_2} + (1+x)K^+$$

where K-feldspar is approximated by orthoclase, and x ($\ll 1$) is a variable dependent on the composition of myrmekite plagioclase. The above reaction involves a net volume loss, and is favored at sites of high normal stress on K-feldspar porphyroclast boundaries during deformation under non-hydrostatic stress (Simpson and Wintsch, 1989). Simpson and Wintsch (1989) inferred that the aqueous K^+ precipitates as K-feldspar in low normal stress regions such as pressure shadows and fractures, as is actually observed in the mylonites studied. The aqueous Na^+ and Ca^{2+} are available from porphyroclast plagioclase replaced by muscovite (e.g. Fig. 4b). A decrease in Na concentration at porphyroclast rims adjacent to myrmekite lobes (e.g. black arrowheads in Fig. 6e) indicates that Na is also supplied from K-feldspar porphyroclast rims via solid-state diffusion, leaving the rims richer in K (e.g. black arrowheads in Fig. 6f). Deflection of fine-grained polymineralic aggregate grains around zoned garnet grains with Ca-rich colorless rims in samples GUM, AML and AUM (e.g. Figs. 7d and 17) suggests the growth of Ca-rich garnet during mylonitization. Provided that myrmekite plagioclase, porphyroclast-rim K-feldspar adjacent to myrmekite lobes, and Ca-rich zoned garnet rims are approximated by albite, orthoclase and grossular, respectively, the following myrmekite-forming reaction is suggested to have occurred in the granite and aplite mylonites along the Hatagawa Shear Zone:

$$\underset{\text{porphyroclast K-feldspar}}{3K_{1-x}Na_xAlSi_3O_8} + \underset{\text{porphyroclast plagioclase}}{3Na_{1-y}Ca_yAl_{1+y}Si_{3-y}O_8} + 2yH_2O \rightarrow \underset{\text{myrmekite plagioclase}}{3(1+x-y)NaAlSi_3O_8} + \underset{\text{myrmekite quartz}}{3ySiO_2} + \underset{\text{porphyroclast-rim K-feldspar}}{(3-3x-2y)KAlSi_3O_8} + \underset{\text{muscovite in plagioclase porphyroclast}}{2yKAl_3Si_3O_{10}(OH)_2} + \underset{\text{Ca-rich garnet rim}}{yCa_3Al_2Si_3O_{12}}$$

where x and y (x, $y \ll 1$) are variables dependent on the compositions of porphyroclast K-feldspar and plagioclase, respectively. x ranges from 0.03 to 0.18, while y ranges from 0.09 to 0.20 in the mylonites studied.

A decrease in Fe_2O_3, MgO and TiO_2 with increasing mylonitization in the granite mylonites (Figs. 13 and 14a) implies breakdown of biotite during mylonitization, because biotite is the only mineral containing these elements in the granite mylonites except for GUM containing garnet. An increase in Fe_2O_3 and TiO_2 in the aplite mylonites (Fig. 14b) may be due to the growth of garnet rim. If so, the above

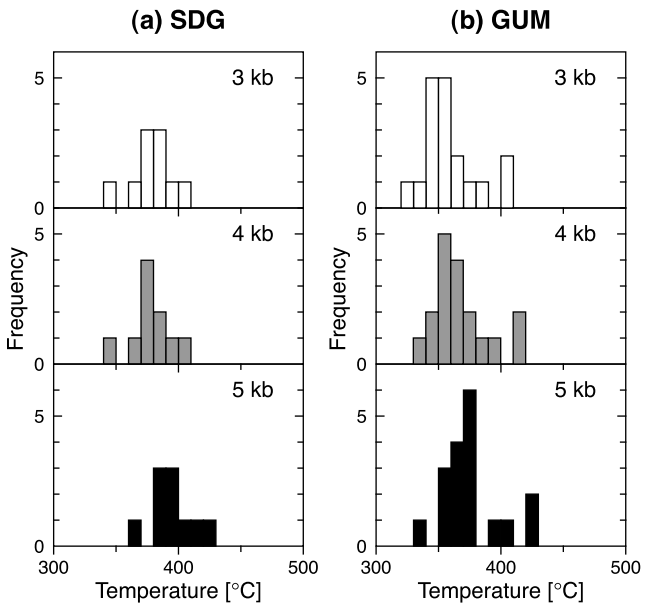

Fig. 18. Calculated temperatures for pressures of 3, 4 and 5 kb applying the two-feldspar thermometry of Whitney and Stormer (1977) to myrmekite plagioclase and adjacent interstitial K-feldspar in two granite samples.

reaction can be rewritten as follows:

$$3\underset{\text{porphyroclast K-feldspar}}{K_{1-x}Na_xAlSi_3O_8} + 6\underset{\text{porphyroclast plagioclase}}{Na_{1-y}Ca_yAl_{1+y}Si_{3-y}O_8}$$

$$+ y\underset{\text{biotite in granite}}{KFe_3AlSi_3O_{10}(OH)_2} + 2yH_2O$$

$$\rightarrow 3(2+x-2y)\underset{\text{myrmekite plagioclase}}{NaAlSi_3O_8} + \underset{\text{myrmekite quartz}}{3ySiO_2}$$

$$+ (3-3x-2y)\underset{\text{porphyroclast-rim K-feldspar}}{KAlSi_3O_8} + \underset{\text{muscovite in plagioclase porphyroclast}}{3yKAl_3Si_3O_{10}(OH)_2}$$

$$+ 2y\underset{\text{garnet rim in aplite mylonite}}{Ca_3Al_2Si_3O_{12}} + 2y\underset{\text{garnet rim in aplite mylonite}}{Fe_3Al_2Si_3O_{12}}$$

In any case, the myrmekite-forming reaction is a hydrated reaction, the water required for which may have been introduced by fracturing during aplite intrusion.

10.4. Temperature estimates

We applied the two-feldspar thermometry of Whitney and Stormer (1977) to the products of myrmekite-forming reaction in samples SDG and GUM[1], i.e. myrmekite plagioclase and its adjacent interstitial K-feldspar, assuming that these two feldspars were in equilibrium during the reaction. The applied thermometry has been calibrated for microcline solid-solutions (Whitney and Stormer, 1977), and is suitable for the pair of plagioclase with low anorthite components and K-feldspar with high orthoclase components as in this study. Temperatures were calculated for 10–20 pairs of two-feldspar compositions assuming pressures of 3, 4 and 5 kb (Fig. 18). Pressures of 3–5 kb correspond to depths of 11.5–19 km in a granite crust with density of 2.66 g/cm^3, and encompass generally accepted pressure conditions of myrmekite-forming reaction and mylonitization. The temperatures calculated for SDG are mostly 370–400 °C, while those for GUM are mostly 340–380 °C, the latter being systematically ≈30 °C lower than the former at the same pressure (Fig. 18). Thus the myrmekite-forming reaction likely occurred in the ultramylonite (GUM) at lower temperatures than in the strongly deformed granite (SDG). Because the myrmekite-forming reaction proceeded with mylonitization as discussed above, the calculated temperatures also represent the temperatures during mylonitization.

Quartz *c*-axis fabrics provide additional information on deformation temperatures. It is well known that *Y*-maximum fabrics such as in sample SDG (Fig. 12a) are common at moderate temperatures (ca. 400–550 °C), while Type I crossed girdle fabrics as in samples GM2 and GUM (Fig. 12c and d) occur at relatively low temperatures (e.g. Schmid and Casey, 1986; Law, 1990; Passchier and Trouw, 1996). In addition, the quartz *c*-axis fabric of sample GM1 (Fig. 12b) likely represents a transition between a *Y*-maximum fabric and a Type I crossed girdle fabric. It follows therefore that the deformation temperature decreases from SDG toward GUM, as does the reaction temperature indicated by two-feldspar thermometry. The quartz *c*-axis fabric transition should have therefore occurred at temperatures of 370–380 °C in the granite mylonites along the Hatagawa Shear Zone, taking account of temperatures estimated for SDG and GUM. These temperatures are consistent with previously reported temperatures of 350–450 °C for the fabric transition between Type I crossed girdles and Type II crossed girdles (Lister 1977) or *Y*-maximum patterns (Takeshita and Wenk, 1988; Sakakibara, 1995).

Ductile shearing along the Hatagawa Shear Zone at 106–86 Ma (Otsuki and Ehiro, 1992) likely occurred during cooling of a granite pluton with a K–Ar biotite age of 114 Ma (Kubo and Yamamoto, 1990), from which our granite and aplite samples were collected. The lower temperatures estimated in the mylonites as compared with those in the surrounding granite may imply that deformation and myrmekite-forming reactions have continued to lower temperatures in the mylonites than in the surrounding granite, probably because of the lower strength of the mylonites.

10.5. Strain localization process

Within the Hatagawa Shear Zone, aplite veins are preferentially mylonitized (Fig. 2a and b). Sample GUM has a modal composition distinct from those of the other granites, but close to those of the aplites (Fig. 8a). Both GUM and aplites contain small amount (≈0.5%) of garnet, which is absent in the other granites, and are rich in K-feldspar (41–47%) and poor in biotite (1–3%) (Fig. 8a). The modal compositions of the aplites indicate that the changes in modal composition during mylonitization are minor (Fig. 8a), and therefore suggest that the differences in

modal composition between GUM and the other granites are largely attributable to initial compositional differences; i.e. GUM may have been more leucocratic than the other granites. GUM also has a bulk chemical composition close to those of the aplites, being rich in SiO_2 and K_2O, poor in CaO, Fe_2O_3 and TiO_2, and absent in MgO (Fig. 13). Thus GUM is aplitic, and may have actually been an aplite.

Fracturing during aplite intrusion may also have introduced water required for the myrmekite-forming reaction in aplite veins and their adjacent granite. Aplite veins are richer in K-feldspar than the surrounding granite (Fig. 8a). Deformation-induced K-feldspar replacement by myrmekite (Simpson and Wintsch, 1989) is therefore more favored during deformation, so that more abundant fine-grained polymineralic aggregates mainly composed of the reaction products are produced. Subsequent reaction softening as well as possible water weakening lead to more enhanced deformation in aplite veins, which promotes further myrmekite-forming reaction. Such a positive feedback of deformation and myrmekite-forming reaction may be responsible for strain localization in aplite veins along the Hatagawa Shear Zone. Provided that GUM is an aplite, the granite mylonites are developed only adjacent to aplite veins in the study area (Fig. 2a and b). The strain localization in aplite veins may also cause the adjacent granite to develop mylonites through the same process as in aplite veins.

10.6. Mass transfer during mylonitization

In contrast to a systematic change in bulk chemical composition with increasing mylonitization in the granites, the change in bulk chemical composition in the aplites is apparently minor (Fig. 13). In particular, CaO, Fe_2O_3, MgO, TiO_2 and P_2O_5 concentrations are apparently constant in the aplites (Fig. 13). This may imply that the changes in bulk chemical composition in the studied granites are not due to mass transfer during mylonitization as previously reported (e.g. O'Hara, 1988; Glazner and Bartley, 1991; Newman and Mitra, 1993; Hippertt, 1998; Streit and Cox, 1998; Bialek, 1999), but rather to initial compositional heterogeneity; i.e. more differentiated granite may have been more intensely mylonitized. O'Hara (1988) has ruled out the latter possibility for the Rector Branch mylonites in North Carolina because enrichments in elements such as Ti, P, Mn and Zr were anomalously high compared with granitic rocks in general. Similar element enrichment has been observed in other granitic mylonites (e.g. Glazner and Bartley, 1991; Newman and Mitra, 1993; Streit and Cox, 1998). In addition, differentiated granites and aplites tend to be depleted rather than enriched in these incompatible elements (cf. Fig. 13 for TiO_2 and P_2O_5), and therefore preferential mylonitization in differentiated granites cannot be applied to the above granitic mylonites. In contrast, the change in bulk chemical composition with increasing mylonitization in the studied granites (Fig. 13) is consistent with that due to differentiation. The modal composition of GM2 intermediate between those of GUM and GM1 (Fig. 8a) may also be due to GM2 having more leucocratic than GM1 but less leucocratic than GUM. Because the granite mylonites are located at the margin of a granite pluton, such a variation in lithology and chemical composition may be possible. Thus strain may have been localized into aplite veins and adjacent leucocratic granite domains in the Hatagawa Shear Zone.

In contrast, relative changes in element concentration in the aplite samples (Fig. 14b) likely indicate mass transfer during mylonitization. It is noteworthy that the changes in element concentration with increasing mylonitization in the aplite samples are opposite to those in the granite samples; i.e. an increase in K_2O and a decrease in CaO, Fe_2O_3, MgO, TiO_2 and P_2O_5 in the granite samples, while a decrease in K_2O and an increase in CaO, Fe_2O_3, TiO_2 and P_2O_5 in the aplite samples (Fig. 14). This may imply a mass transfer of these elements between the aplite mylonites and their adjacent granite mylonites, although the sink for MgO depleted from the granite mylonites remains unknown. The transfer of aqueous K^+ enables precipitation of K-feldspar in fracture fillings, pressure shadows and fine-grained polymineralic aggregates. Possible breakdown of plagioclase and biotite in the granite mylonites and Ca-rich garnet growth in the aplite mylonites may also represent such mass transfer between the granite and aplite mylonites. Thus the granite mylonites in the Hatagawa Shear Zone may have not been initially leucocratic, but may have become leucocratic by mass transfer during mylonitization.

Initial compositional heterogeneity cannot explain a subtle but systematic change in element concentration with increasing mylonitization in the aplite mylonites, whereas mass transfer between the granite and aplite mylonites has difficulty in explaining the absence of MgO in the aplite mylonites. Without additional data, neither of the above two possibilities can be excluded at present.

10.7. Deformation mechanisms and rheological implications

Microstructural evidence for crystal plastic deformation and dynamic recrystallization of quartz (e.g. Figs. 3c and 4e) and development of quartz *c*-axis fabrics (Fig. 12) in both the non-mylonitic and mylonitic granites indicate that the quartz aggregates were deformed by dislocation creep. Because deformation of the non-mylonites is represented by crystal plastic deformation and dynamic recrystallization of quartz, their rheology is likely controlled by quartz deforming by dislocation creep. In contrast, the rheology of mylonites containing abundant fine-grained polymineralic aggregates (up to 60–80 mode% in the ultramylonites) (Fig. 8b) must be controlled by the fine-grained polymineralic aggregate. However, the deformation mechanism and rheology of the fine-grained polymineralic aggregate remain unknown at present, and need to be further studied.

The fine-grained polymineralic aggregates of plagioclase + K-feldspar + quartz ± biotite in quartz–feldspar mylonites from southern California and central Australia have been inferred to have deformed by grain boundary sliding, because of their very small grain size (≤10 μm), almost random quartz *c*- and *a*-axes fabrics, misorientation between adjacent quartz grains not attributable solely to dislocation activity, and grain boundaries decorated with voids (Behrmann and Mainprice, 1987; Fliervoet et al., 1997). The fine-grained polymineralic aggregate in this study may be too coarse-grained (≤50 μm) for grain boundary sliding to have been active under given deformation conditions. However, it should be noted that the fine-grained polymineralic aggregates in the ultramylonites are a rather homogeneous mixture of myrmekite lobes, their interstitial K-feldspar grains isolated from porphyroclast rims or precipitated from solution, quartz grains derived from quartz ribbons, K-feldspar grains derived from K-feldspar ribbons, and biotite grains derived from aggregate biotite (e.g. Figs. 6c and d and 7c). A significant amount of grain boundary sliding may be required to produce such a homogeneous mixture. In addition to data on crystallographic fabrics, misorientation distributions between adjacent grains, and intra- and inter-crystalline defect structures as described by Behrmann and Mainprice (1987) and Fliervoet et al. (1997), data on spatial distribution of constituent minerals may also provide useful information on the activity of grain boundary sliding.

11. Conclusions

From the changes with progressive mylonitization in microstructure, modal composition, grain size, quartz aggregate shape, quartz *c*-axis fabric, and bulk and mineral chemistries, the following conclusions are drawn related to strain localization in the granite and aplite mylonites along the Hatagawa Shear Zone of NE Japan.

1. Strain is localized into narrow (10 cm–3 m) zones of mylonites with shear strains larger than 1.9.
2. With increasing mylonitization of both granite and aplite, the modal content of feldspar porphyroclasts as well as their grain size decrease, while the modal content of fine-grained (≤50 μm) polymineralic aggregate made up of plagioclase, K-feldspar, quartz and biotite increases up to 60–80% in the granite and aplite ultramylonites. The fine-grained polymineralic aggregates are formed by mixing of myrmekite lobes and their interstitial K-feldspar isolated from porphyroclast rims and/or precipitated from solution, with minor amounts of quartz, biotite and K-feldspar grains incorporated from their monomineralic aggregates. An increasing amount of fine-grained polymineralic aggregate with increasing mylonitization implies that the myrmekite-forming reaction proceeded with mylonitization.
3. Deformation-induced myrmekite lobes (Simpson and Wintsch, 1989) are ubiquitously developed around K-feldspar porphyroclasts along their boundaries subparallel to mylonitic foliation, and are formed by either of the following hydrated reactions during mylonitization:

$$\underset{\text{porphyroclast K-feldspar}}{3K_{1-x}Na_xAlSi_3O_8} + \underset{\text{porphyroclast plagioclase}}{3Na_{1-y}Ca_yAl_{1+y}Si_{3-y}O_8} + 2yH_2O$$
$$\rightarrow \underset{\text{myrmekite plagioclase}}{3(1+x-y)NaAlSi_3O_8} + \underset{\text{myrmekite quartz}}{3ySiO_2}$$
$$+ \underset{\text{porphyroclast-rim K-feldspar}}{(3-3x-2y)KAlSi_3O_8}$$
$$+ \underset{\text{muscovite in plagioclase porphyroclast}}{2yKAl_3Si_3O_{10}(OH)_2} + \underset{\text{Ca-rich garnet rim}}{yCa_3Al_2Si_3O_{12}}$$

or

$$\underset{\text{porphyroclast K-feldspar}}{3K_{1-x}Na_xAlSi_3O_8} + \underset{\text{porphyroclast plagioclase}}{6Na_{1-y}Ca_yAl_{1+y}Si_{3-y}O_8}$$
$$+ \underset{\text{biotite in granite}}{yKFe_3AlSi_3O_{10}(OH)_2} + 2yH_2O$$
$$\rightarrow \underset{\text{myrmekite plagioclase}}{3(2+x-2y)NaAlSi_3O_8} + \underset{\text{myrmekite quartz}}{3ySiO_2}$$
$$+ \underset{\text{porphyroclast-rim K-feldspar}}{(3-3x-2y)KAlSi_3O_8}$$
$$+ \underset{\text{muscovite in plagioclase porphyroclast}}{3yKAl_3Si_3O_{10}(OH)_2}$$
$$+ 2yCa_3Al_2Si_3O_{12} + \underset{\text{garnet rim in aplite mylonite}}{2yFe_3Al_2Si_3O_{12}}$$

where x and y ($x, y \ll 1$) are variables dependent on the compositions of porphyroclast K-feldspar and plagioclase, respectively. Water required for the above reactions may have been introduced by fracturing during aplite intrusion.
4. Both two-feldspar thermometry and quartz *c*-axis fabrics indicate that the temperatures of deformation and the myrmekite-forming reaction decreased from the surrounding granite (370–400 °C) to the ultramylonite (340–380 °C). This suggests that deformation and the myrmekite-forming reaction have continued to lower temperatures in the ultramylonites than in the surrounding granite, probably because of lower strength of the mylonites containing abundant fine-grained polymineralic aggregates.
5. Modal and bulk chemical compositions of the granites and aplites indicate that mylonites are preferentially developed in aplite veins richer in K-feldspar than the surrounding granite. Deformation-induced K-feldspar replacement by myrmekite is then more favored during deformation to produce more abundant fine-grained polymineralic aggregates. Subsequent reaction softening leads to more enhanced deformation, which promotes further myrmekite-forming reaction. Such a positive

feedback of deformation and myrmekite-forming reaction in aplite veins is responsible for strain localization in aplite veins and adjacent granite along the Hatagawa Shear Zone, and may be a common process in ductile shear zones of the granitic middle crust.

6. A systematic change in modal and bulk chemical compositions in granite with increasing mylonitization may be due to either initial compositional heterogeneity or mass transfer during mylonitization. In the former case, strain has been localized into aplite veins and their adjacent leucocratic granite domains in the Hatagawa Shear Zone. But in the latter case, granite mylonites in the Hatagawa Shear Zone have become leucocratic by mass transfer during mylonitization.

Acknowledgments

We thank M. Enami, Y. Hiroi, T. Ito and T. Nishiyama for discussions and suggestions, N. Shigematsu for providing his geologic map in press, T. Okudaira for advice on temperature calculations, R. Heilbronner for providing her LGB macro for NIH Image used in grain-size analysis, M. Furusho, S. Miyoshi and H. Yoshida for assisting with EPMA analyses, and H. Yoshida for assisting with XRF analysis. We also thank R. Law, K. O'Hara and R. Wintsch for helpful reviews, and D. Fisher for editorial handling. This study was supported by Grant 07454120 from the Ministry of Education, Science and Culture of Japan to K. Kanagawa.

References

Behrmann, J.H., Mainprice, D., 1987. Deformation mechanisms in a high-temperature quartz–feldspar mylonite: evidence for superplastic flow in the lower continental crust. Tectonophysics 140, 297–305.

Berthé, D., Choukroune, P., Gapais, D., 1979. Orientations préférentielles du quartz et orthogneissification progressive en régime cisaillant: l'exemple du cisaillant sud-armoricain. Bulltin de Minéralogie 102, 265–272.

Bialek, D., 1999. Chemical changes associated with deformation of granites under greenschist facies conditions: the example of the Zawidów Granodiorite (SE Lusatian Granodiorite Complex, Poland). Tectonophysics 303, 251–261.

Fliervoet, T., White, S.H., Drury, M.R., 1997. Evidence for dominant grain-boundary sliding deformation in greenschist- and amphibolite-grade polymineralic ultramylonites from the Redbank Deformed Zone, Central Australia. Journal of Structural Geology 19, 1495–1520.

Gibson, R.G., 1990. Nucleation and growth of retrograde shear zones: an example from the Needle Mountains, Colorado, USA. Journal of Structural Geology 12, 339–350.

Glazner, A.F., Bartley, J.M., 1991. Volume loss, fluid flow and state of strain in extensional mylonites from the central Mojave Desert, California. Journal of Structural Geology 13, 587–594.

Guermani, A., Pennacchioni, G., 1998. Brittle precursors of plastic deformation in a granite: an example from the Mont Blanc massif (Helvetic, western Alps). Journal of Structural Geology 20, 135–148.

Hippertt, J.F., 1998. Breakdown of feldspar, volume gain and lateral mass transfer during mylonitization of granitoid in a low metamorphic grade shear zone. Journal of Structural Geology 20, 175–193.

Koshiya, S., 1988. Quartz c-axis fabric and microstructure in mylonite—an application to the Hatakawa Shear Zone, northeast Japan. Journal of the Tectonic Research Group of Japan 33, 13–32.

Kubo, K., Yamamoto, T., 1990. Cretaceous intrusive rocks of the Haramachi district, eastern margin of the Abukuma Mountains—petrology and K–Ar age. Journal of the Geological Society of Japan 96, 731–743.

Kubo, K., Yanagisawa, Y., Yoshioka, T., Yamamoto, T., Takizawa, F., 1990. Geologic map of the Haramachi and Omika district. Geological Survey of Japan Quadrangle Series Map, scale 1:50,000.

Law, R.D., 1990. Crystallographic fabrics: a selective review of their applications to research in structural geology. In: Knipe, R.J., Rutter, E.H. (Eds.), Deformation Mechanisms, Rheology and Tectonics. Geological Society Special Publication 54, pp. 335–352.

Lister, G.S., 1977. Discussion: crossed girdle c-axis fabrics in quartzites plastically deformed by plane strain and progressive simple shear. Tectonophysics 39, 51–54.

Malavieille, J., Ritz, J.F., 1989. Mylonitic deformation of evaporites in décollements: examples from the Southern Alps, France. Journal of Structural Geology 11, 583–590.

Newman, J., Mitra, G., 1993. Lateral variations in mylonite zone thickness as influenced by fluid–rock interactions, Linville Falls fault, North Carolina. Journal of Structural Geology 15, 849–863.

O'Hara, K., 1988. Fluid flow and volume loss during mylonitization: an origin for phyllonite in an overthrust setting, North Carolina, USA. Tectonophysics 156, 21–36.

Otsuki, K., Ehiro, M., 1992. Cretaceous left-lateral faulting in Northeast Japan and its bearing on the origin of geologic structure of Japan. Journal of the Geological Society of Japan 98, 1097–1112.

Passchier, C.W., 1982. Pseudotachylyte and the development of ultramylonite bands in the Saint-Balthélemy Massif, French Pyrenees. Journal of Structural Geology 4, 69–79.

Passchier, C.W., Trouw, R.A.J., 1996. Microtectonics, Springer, Heidelberg.

Poirier, J.P., 1980. Shear localization and shear instability in materials in the ductile field. Journal of Structural Geology 2, 135–142.

Sakakibara, N., 1995. Structural evolution of multiple ductile shear zone system in the Ryoke belt, Kinki Province. Journal of Science of the Hiroshima University: Series C 10, 267–332.

Schmid, S.M., 1975. The Glarus overthrust: field evidence and mechanical model. Eclogae Geologae Helvetiae 68, 247–280.

Schmid, S.M., Casey, M., 1986. Complete fabric analysis of some commonly observed quartz c-axis patterns. In: Hobbs, B.E., Heard, H.C. (Eds.), Mineral and Rock Deformation: Laboratory Studies. American Geophysical Union Geophysical Monograph 36, pp. 263–286.

Segall, P., Simpson, C., 1986. Nucleation of ductile shear zones on dilatant fractures. Geology 14, 56–59.

Shigematsu, N., 1999. Dynamic recrystallization in deformed plagioclase during progressive shear deformation. Tectonophysics 305, 437–452.

Shigematsu, N., Tanaka, H., 2000. Dislocation creep of fine-grained recrystallized plagioclase under low-temperature conditions. Journal of Structural Geology 22, 65–79.

Shigematsu, N., Yamagishi, H., 2002. Quartz microstructures and deformation conditions in the Hatagawa shear zone, north-east Japan. The Island Arc 11, 45–60.

Shimamoto, T., Ikeda, Y., 1976. A simple algebraic method for strain estimation from deformed ellipsoidal objects—1. Basic theory. Tectonophysics 36, 315–337.

Sibson, R.H., 1977. Fault rocks and fault mechanisms. Journal of the Geological Society of London 133, 191–213.

Simpson, C., 1985. Deformation of granitic rocks across the brittle–ductile transition. Journal of Structural Geology 7, 503–511.

Simpson, C., Wintsch, R.P., 1989. Evidence for deformation-induced

K-feldspar replacement by myrmekite. Journal of Metamorphic Geology 7, 261–275.

Streit, J.E., Cox, S.F., 1998. Fluid infiltration and volume change during mid-crustal mylonitization of Proterozoic granite, King Island, Tasmania. Journal of Metamorphic Geology 16, 197–212.

Takagi, H., Goto, K., Shigematsu, N., 2000. Ultramylonite bands derived from cataclasite and pseudotachylyte in granites, northeast Japan. Journal of Structural Geology 22, 1325–1339.

Takeshita, T., Wenk, H.-R., 1988. Plastic anisotropy and geometrical hardening in quartzites. Tectonophysics 149, 345–361.

Tullis, J., Yund, R.A., 1985. Dynamic recrystallization of feldspar: a mechanism for ductile shear zone formation. Geology 13, 238–241.

Tullis, J., Dell'Angelo, L., Yund, R.A., 1990. Ductile shear zones from brittle precursors in feldspathic rocks: the role of dynamic recrystallization. In: Duba, A.G., Durham, W.B., Handin, J.W., Wang, H.F. (Eds.), The Brittle–Ductile Transition in Rocks. American Geophysical Union Geophysical Monograph 56, pp. 67–81.

Tullis, J., Snoke, A.W., Todd, V.R., 1982. Significance and petrogenesis of mylonitic rocks. Geology 10, 227–230.

Vauchez, A., 1987. The development of discrete shear-zones in a granite: stress, strain and changes in deformation mechanisms. Tectonophysics 133, 137–156.

Wheeler, J., 1984. A new plot to display the strain of elliptical markers. Journal of Structural Geology 6, 417–423.

White, S.H., Burrows, S.E., Carreras, J., Shaw, N.D., Humphreys, F.J., 1980. On mylonites in ductile shear zones. Journal of Structural Geology 2, 175–187.

Whitney, J.A., Stormer, J.C. Jr, 1977. The distribution of $NaAlSi_3O_8$ between coexisting microcline and plagioclase and its effect on geothermometric calculations. American Mineralogist 62, 687–691.

Yoshida, H., Takahashi, N., 1997. Chemical behavior of major and trace elements in the Horoman mantle diapir, Hidaka belt, Hokkaido, Japan. Journal of Mineralogy, Petrology and Economic Geology 92, 391–409.